Comparative Medicine
Copyright 2014
by the American Association for Laboratory Animal Science

Vol 64, No 3
June 2014
Pages 211–10

Case Report

Use of ^{18}F-Fluorodeoxyglucose Positron Emission Tomography–Computed Tomography to Aid in Diagnosing Intestinal Adenocarcinoma in 2 Rhesus Macaques (*Macaca mulatta*)

Debra J Caporizzo,[1] Anna E Kwiatkowski,[1] Ming-Kai Chen,[2] Amanda P Beck,[1] Carmen J Booth,[1] Caroline Zeiss,[1] Peter C Smith,[1] Jodi A Carlson Scholz,[1] and Steven R Wilson[1,*]

Two aged female rhesus macaques (*Macaca mulatta*) presented with weight loss and intermittent inappetence. The signalment and constellation of clinical signs led clinicians to suspect the presence of intestinal adenocarcinoma. Because of each animal's advanced age and inconclusive radiographic findings, a noninvasive diagnostic tool was preferred over exploratory laparotomy to assist in determining a diagnosis. Consequently, 2-[^{18}F]fluoro-2-deoxy-d-glucose (FDG) positron emission tomography–CT (FDG-PET–CT) was chosen to aid in confirming a suspicion of gastrointestinal adenocarcinoma in both animals. FDG is a glucose analogue labeled with fluorine-18 and is taken up by highly metabolically active cells, as observed in many cancers. Tomography revealed an annular constriction of the small intestine with focal FDG uptake in one animal, and an FDG avid transmural mass in the ascending colon of the second animal. Necropsy later confirmed both sites to be adenocarcinomas. This report supports the use of FDG-PET–CT as an adjunct to conventional radiography in the diagnosis of intestinal adenocarcinoma in nonhuman primates.

Abbreviations: FDG, 2-[^{18}F]fluoro-2-deoxy-d-glucose; PET, positron emission tomography.

The noninvasive imaging modality 2-[^{18}F]fluoro-2-deoxy-d-glucose positron emission tomography-computed tomography (FDG-PET–CT) is used primarily for the detection and staging of cancer and for the assessment of therapeutic response.[28] This modality also is useful for the identification of some infectious and inflammatory diseases, as demonstrated in the recent report of intense FDG uptake in a case of pneumonia in a miniature pig.[14] Furthermore, FDG-PET–CT has been helpful in the detection and monitoring of inflammatory bowel disease and complicating infections of the gastrointestinal tract.[28]

PET detects the three-dimensional distribution of radioactivity based on the annihilation photons emitted by radiotracers labeled with positron-emitting radionuclides, such as ^{18}F-labeled FDG. In this manner, PET enables noninvasive assessment of biochemical processes. In contrast, CT uses X-rays to generate high-resolution images, allowing clear visualization of anatomic structures. In PET–CT, both the multidetector CT apparatus and the PET detectors are mounted in the same scanner, one behind the other. The PET data are superimposed on the CT data (coregistration), enabling precise anatomic localization of FDG activity.[29] Combining PET imaging with CT allows the fusion of functional and anatomic information acquired almost simultaneously, facilitating the visualization and localization of metabolic information noninvasively.

Intestinal adenocarcinoma is a substantial cause of morbidity and mortality in aged rhesus macaques.[25,26,30] Rhesus macaques often are maintained on long term-studies, resulting in a population of animals exhibiting morbidities associated with advanced age.[20,25,26] As the age of the animals in our care advances, so too must our diagnostic capabilities advance. Here we report the use of a noninvasive method, FDG-PET–CT, to support the diagnosis of intestinal adenocarcinoma in 2 aged rhesus macaques. We describe the physics of PET, biochemical rationale for the use of FDG, and pitfalls of interpretation.

Case Reports

The first of the 2 cases we present is that of a 27-y-old reproductively intact female rhesus macaque (*Macaca mulatta*) presented to veterinary services with a history of intermittent inappetence and occasional vomiting. Macaque 1 was a retired breeder involved in noninvasive cognitive-testing experiments to examine the interactions between cortical and subcortical structures and their dependence on dopamine. All experimentation was approved by the Yale University IACUC. The macaque was pair-housed indoors in an AAALAC-accredited facility and fed a commercial diet (Primate Chow 8714, Harlan Teklad, Madison, WI), supplemented daily with a variety of fruits and vegetables. She was seronegative for simian T- cell leukemia virus types 1 and 2, simian retro-

Received: 20 Aug 2013. Revision requested: 07 Oct 2013. Accepted: 12 Nov 2013.
[1]Section of Comparative Medicine and [2]Department of Diagnostic Radiology, Yale University School of Medicine, New Haven, Connecticut.
[*]Corresponding author. Email: steven.r.wilson@yale.edu

virus type D, SIV, *Macacine herpesvirus 1* (B virus), and measles. In addition, she tested negative for tuberculosis by semiannual intradermal tuberculin testing and annual in vitro tuberculin immunoassay. All examinations were performed under ketamine sedation (10 mg/kg IM).

During a semiannual examination in October 2011, macaque 1 was noted to have palpably thickened intestines and a weight loss of 1 kg over the past year. Results of a routine CBC and serum biochemistry profile were unremarkable. Over the next 3 mo, she intermittently refused treats and occasionally vomited. A recheck physical examination revealed hypothermia (96.4 °F), dehydration, and weight loss of 2 kg (approximately 20% of body weight) since her semiannual exam 3 mo prior. Abdominal palpation demonstrated a doughy abdomen with firm ropey intestines. Thoracic and abdominal radiographs were performed to rule out neoplasia and metastatic disease. Concurrently, intravenous fluids were administered, and blood samples collected for a CBC and serum biochemistry profile. Thoracic radiographs were unremarkable. Abdominal radiographs revealed a fluid-distended stomach and proximal small intestine, suggesting a possible obstruction distally (Figure 1 A and B). Hematology results were unremarkable except for a moderate neutrophilia. Results of the serum biochemistry profile revealed azotemia, hyponatremia, and hyperkalemia (Na:K, less than 21; Table 1).

Differential diagnoses for the azotemia in macaque 1 included dehydration, renal disease, and gastrointestinal bleeding. Causes of hyperkalemia with hyponatremia include severe gastrointestinal disease, renal failure, and hypoadrenocorticism. Differential diagnoses for obstructive intestinal disease in rhesus macaques include endometriosis, adhesions, tumor, foreign body, bezoar, and functional ileus. Although a discrete mass could not be palpated, a malignant tumor was the likely suspect in this elderly animal. All blood chemistry abnormalities resolved with fluid therapy, and macaque 1 demonstrated significant clinical improvement. However, her appetite again began to wax and wane over the next few weeks. In addition, vomiting increased in frequency and character, at one point becoming fetid. Exploratory surgery was considered but dismissed in favor of less invasive diagnostics. Because commonly used imaging modalities provide only morphologic information, FDG-PET–CT was chosen to assist in identifying the nature of the suspected obstruction.

The macaque was scanned (Biograph mCT, Siemens, Deerfield, IL) at the Yale University PET Center. This machine is a whole-body PET–CT scanner that acquires 109 PET slices with resolution of approximately 5 × 5 × 5 mm and 128-slice CT. A series of 3 scans was performed: a positioning topographic scan, a CT scan for attenuation correction and anatomic localization, and a PET scan. After the topogram and CT scan, 5.62 mCi (208 MBq) of ^{18}F-FDG was administered intravenously, followed by a saline flush. After allowing the PET radiopharmaceutical to localize for 55 min, a whole-body PET scan was acquired.

Imaging revealed a small-intestinal annular constriction with focally intense FDG uptake at the site (Figure 2 A, B, and D). The stomach and proximal bowel were fluid-distended as a result of the almost complete distal obstruction (Figure 2 A and B). Given her advanced age and stage of disease, macaque 1 was euthanized.

Postmortem examination of macaque 1 revealed the presence of a fluid-distended stomach and bowel, anterior to a focal annular stricture in the proximal jejunum. The cause of the constriction was a 1 cm × 2 cm, circumferential, transmural, proliferative, infiltrative mass extending from the lumen to the adjacent mesenteric adipose (Figure 3 A and B). The lumen at the stricture site was 1 to 2 mm (Figure 3 B). Microscopically, the tumor was composed of columnar epithelial cells with one or more large pleomorphic nuclei, one or more prominent nucleoli, and an increased nuclear-to-cytoplasmic ratio. Neoplastic cells formed disorganized glands surrounded by abundant fibrous connective tissue (desmoplasia) admixed with numerous leukocytes (Figure 3 D). Also noted were 1 to 3 mitotic figures per high-power field. The final diagnosis was a well-differentiated and infiltrative, circumferential adenocarcinoma of the proximal jejunum. No metastases were detected.

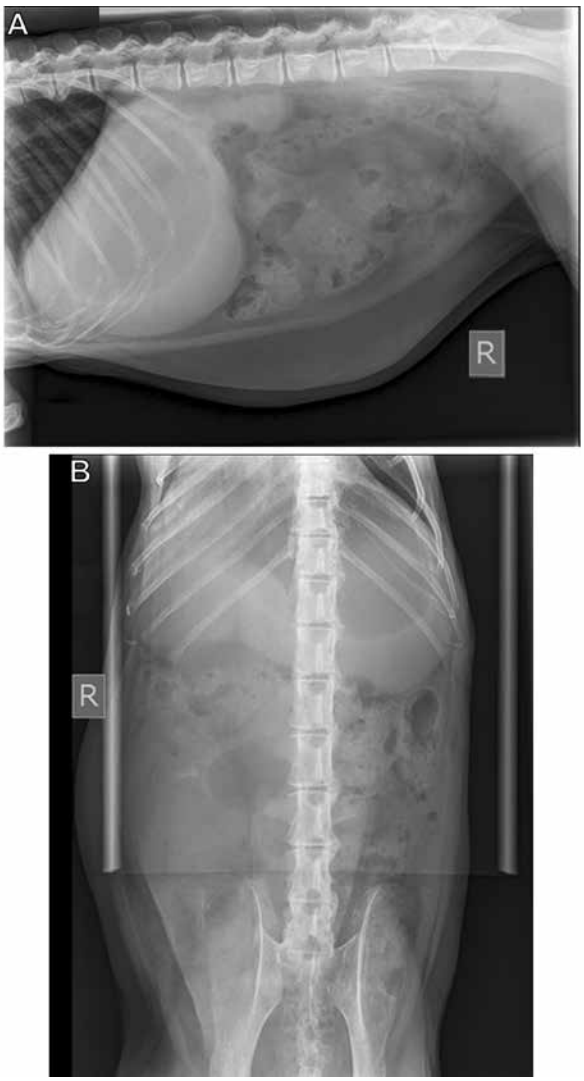

Figure 1. Abdominal radiographs of rhesus macaque 1. (A) Right lateral and (B) ventrodorsal views demonstrate gaseous and fluid distention of the stomach and proximal small intestines suggestive of obstructive disease.

The second case involves a 26-y-old, ovariectomized female rhesus macaque that presented with multiple, firm, nodular, cranial abdominal masses during routine veterinary evaluation. Prior to this presentation, macaque 2 was a retired breeder used for cognitive-function studies. All regulatory, husbandry, and serologic features were similar to those for case 1.

Table 1. Clinically significant hematology and serum chemistry results for macaques 1 and 2.

	Macaque 1	Macaque 2	Reference range
RBC, $\times 10^6$/μL	6.5	**4.3**	5.8–6.9
Hct, %	46.1	**25.0**	41.3–47.5
MCV, fL	71	**58**	67–73
MCH, pg	23.5	**17.4**	21.9–23.9
MCHC, g/dL	33.0	**30.0**	32.5–33.5
WBC, $\times 10^3$/μL	9.9	**3.4**	5.3–11.3
Neutrophils, $\times 10^3$/μL	**85.1 (86%)**	**23.1 (68%)**	39–63
Lymphocytes, $\times 10^3$/μL	**7.9 (8%)**	**8.1 (24%)**	26–50
Monocytes, 10^3/μL	**1.0 (5%)**	**0.7 (2%)**	4–10
Eosinophils, 10^3/μL	1.0 (1%)	2.0 (6%)	1–7
Platelets, $\times 10^3$/μL	**553**	**898**	246–456
Total protein, g/dL	6.7	**5.8**	6.5–7.9
Albumin, g/dL	3.7	**2.8**	3.4–4.4
Sodium, mEq/L	**129**	146	145–151
Potassium, mEq/L	**6.2**	4.1	4.6–5.8

Blood was sampled near the time of imaging. Abnormal values are in boldface.

[a]Reference ranges for geriatric female macaques obtained from the Association of Primate Veterinarians Nonhuman Primate Formulary (http://primateveterinarians.org/pub_downloads.aspx).

In 2011, a firm, lobulated cranial abdominal mass (approximately 5 cm × 5 cm × 5 cm) was palpated during a routine physical examination of macaque 2. Abdominal radiographs revealed a soft-tissue opacity that appeared to be associated with intestine. The primary differential diagnoses at this time were adhesions, diverticulosis, and gastrointestinal adenocarcinoma. Exploratory surgery was considered, but the lack of clinical signs allowed additional monitoring of the macaque without interference with her experimental use. Serial physical examinations throughout the year confirmed that the abdominal mass had remained unchanged.

In early 2012, abdominal palpation of macaque 2 revealed a second irregular, round mass (1.5 cm × 2 cm) adjoined to that previously noted several months earlier. Despite the apparent progression of disease, the macaque maintained a healthy weight and body condition. Additional workup included recheck survey abdominal and thoracic radiographs and ultrasound-guided fine-needle aspiration of the mass. Abdominal radiographs demonstrated a diffusely enlarged and dilated colon (Figure 4 A and B). Ultrasonography confirmed that the cranial abdominal masses were associated with the intestines (Figure 5 A and B), but the cytology of the fine-needle aspirate was nondiagnostic. Thoracic radiographs were negative for evidence of metastatic lesions. A CBC and serum biochemistry profile revealed hypoalbuminemia, lymphopenia, a microcytic, hypochromic anemia, and thrombocytosis (Table 1). Multiple fecal occult blood samples were negative. Physical exam findings, hematology and blood chemistry results, and imaging were highly suggestive of an intestinal malignancy, with adenocarcinoma being the most likely.

In light of the findings from macaque 1, FDG-PET–CT again was chosen to assist with diagnosis. Macaque 2 was scanned by using the same materials and methods as in case 1. Imaging revealed an FDG-avid transmural mass that partially obstructed the proximal colon (Figure 6 A, B, and D). Less-intense, diffuse FDG uptake was noted throughout the proximal bowel (Figure 6 A).

In view of the macaque's guarded prognosis for long-term survival, surgical resection was not attempted. Despite her disease, macaque 2 displayed no outward signs of illness and continued to test and eat well over the next 6 mo; she then experienced rapid weight loss and inappetence over a 7-d period. Because of this rapid decline and her presumptive diagnosis of malignancy, macaque 2 was euthanized.

Necropsy revealed a 4.5 cm × 4.5 cm × 5 cm, firm, multinodular, transmural mass within the proximal colon just distal to the cecum. The mass was accompanied by marked desmoplasia resulting in almost complete obstruction of the colonic lumen and leading to marked dilation of the proximal intestinal tract (Figure 7 A and B). Multiple focal diverticula were noted on cut section (Figure 7 B). Also noted was a focus (diameter, 1 cm) of ulceration within the mass. Histology of the mass revealed a markedly expanding, transmural, and infiltrative neoplasm within the colonic wall (Figure 7 C). Histologically, the colonic mass was composed of neoplastic cells forming tubules and acini embedded in abundant fibrous connective tissue (Figure 7 D). Neoplastic cells were polygonal with indistinct cell borders and moderate amounts of pale eosinophilic cytoplasm. Anisocytosis and anisokaryosis were moderate, and mitotic figures were prominent. The neoplasm extended into the adjacent mesentery where it was admixed with abundant granulation tissue, necrotic cell debris and mixed leukocytes.

Additional nodules were noted within the lung and liver. Two raised umbilicated nodules (maximal diameter, 0.7 cm) were present in the right caudal lung lobe. Multifocally, the pulmonary parenchyma was replaced by an unencapsulated, poorly demarcated neoplasm composed of tubules and acini of neoplastic cells in a fibrovascular stroma. Neoplastic cells had similar features to those of the colonic mass and frequently surrounded mucin and necrotic cell debris. In addition, a similar focal nodule (diameter, 0.3 cm) was noted within the liver. Focally, the hepatic parenchyma was replaced by an unencapsulated, poorly demarcated neoplasm composed of cords and acini of neoplastic cells in a moderate amount of fibrovascular stroma. Neoplastic cells exhibited similar features to those in the colonic mass. Final pathologic diagnosis was a poorly demarcated and infiltrative adenocarcinoma within the proximal colon with metastases to the lung and liver.

Discussion

Intestinal adenocarcinomas are slow-growing but aggressive, locally invasive tumors. Metastasis commonly involves regional lymph nodes, liver, and lungs, as shown in the second case we reported here. Metastasis to the liver is most common, due to portal drainage. Grossly, early tumors may appear as firm thickenings of the wall of the intestine. Ultimately, the lesion spreads circumferentially through submucosal or serosal circular lymphatics to produce an annular lesion. The fibrous stroma of the tumor results in constriction and narrowing of the bowel lumen. As mucosal spread occurs, the muscular wall is invaded and the tumor, at this stage, may extend to the serosa and mesentery.[27]

The most consistent clinical signs of intestinal adenocarcinoma in rhesus macaques are anorexia and weight loss.[20,25,30] Both

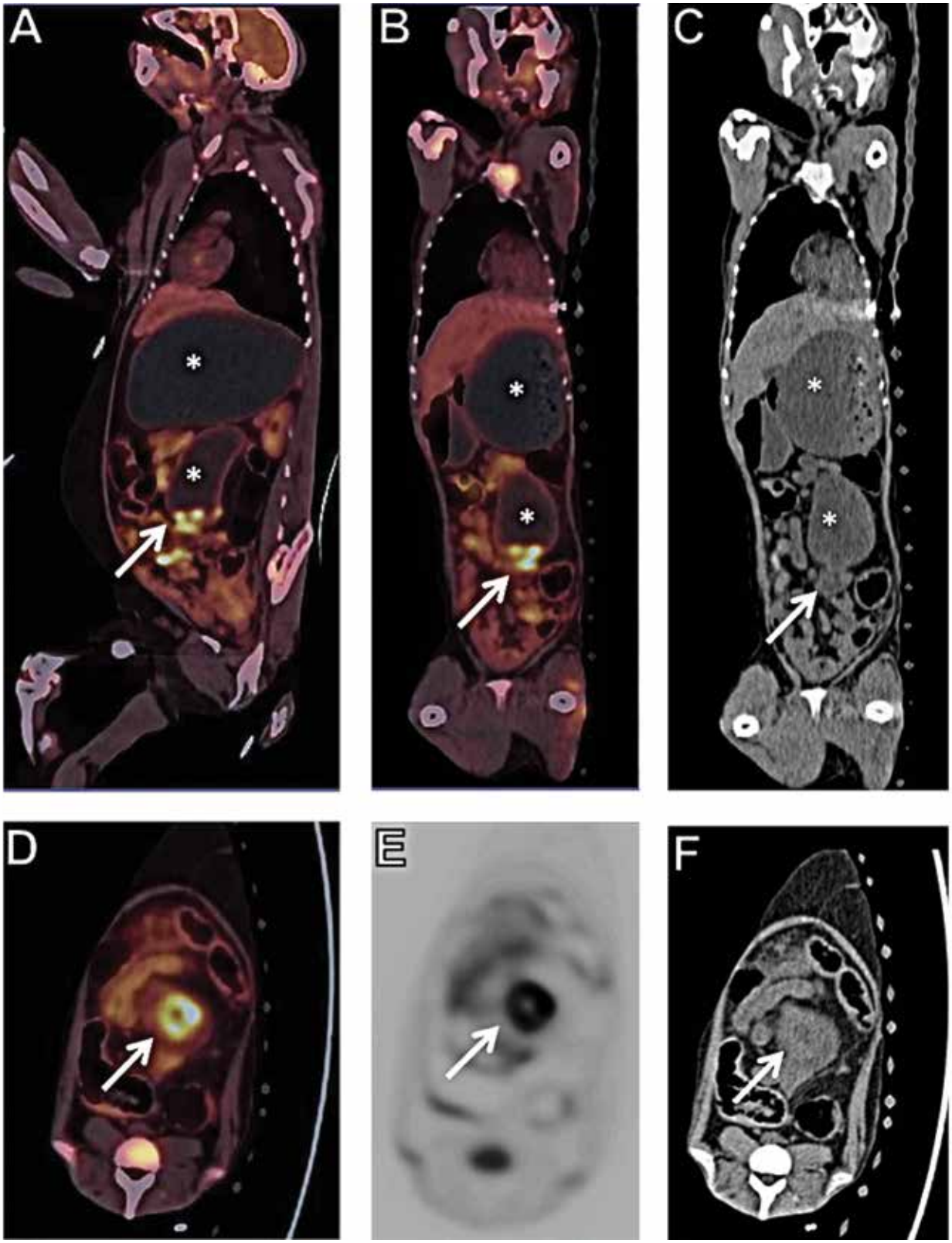

Figure 2. Whole-body FDG-PET–CT, macaque 1. There is focal intense FDG uptake (arrows) noted in a circular transmural mass involving small bowel. The mass causes near-complete obstruction of the lumen, with marked dilation of the proximal small bowel loop and stomach (*). Less intense physiologic FDG activity is present in the brain, liver, and bone marrow. PET–CT (A) sagittal, (B) coronal, and transaxial (D) views; CT (C) coronal and (F) transaxial views; (E) FDG-PET transaxial view.

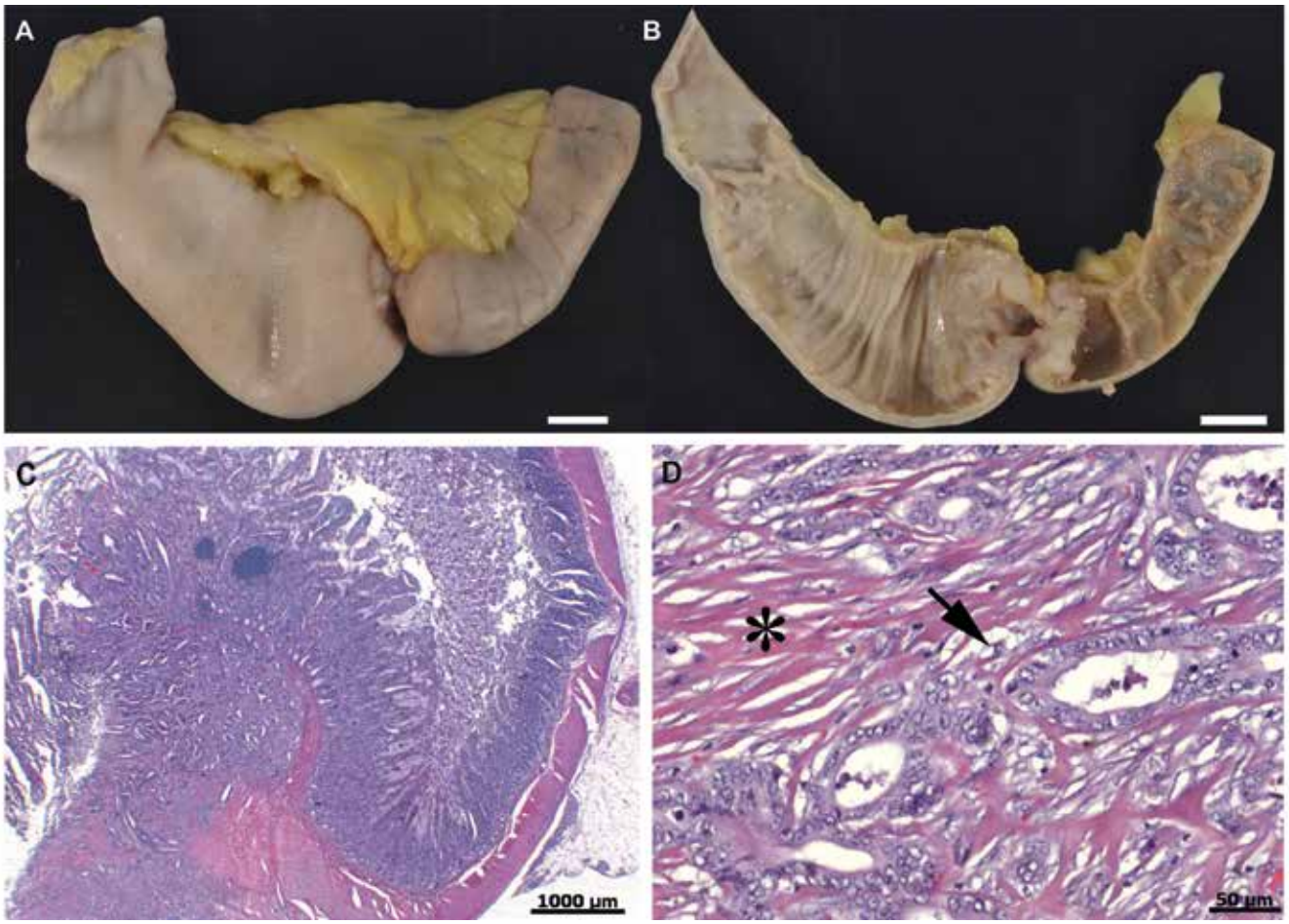

Figure 3. Gross and histologic images of intestinal mass from macaque 1. Fixed (A) intact and (B) sagittal sections through a focal stricture in the proximal jejunum at 10 cm from the pylorus. Maximal distention of the duodenum and jejunum proximal to the stricture was approximately 4 cm in diameter. The lumen at the site of the stricture is 1to 2 mm (arrow). Scale bar, 1 cm. (C) Histology from the stricture site demonstrates a transmural proliferative and diffuse infiltrative mass. (D) Higher (40×) magnification reveals the mass to be composed predominantly of columnar epithelial cells with one or more large pleomorphic nuclei, one or more prominent nucleoli with an increased nuclear to cytoplasmic ratio. Neoplastic cells form disorganized glands (arrow) and are surrounded by abundant amounts of fibrous connective tissue (*, desmoplasia) admixed with numerous inflammatory cells (lymphocytes, plasma cells, macrophages, and neutrophils). Mitotic figures vary from 1to 3 per high-power field. Hematoxylin and eosin stains.

animals reported here experienced these consistent but vague signs. In humans, symptoms such as vomiting and change in bowel habits typically reflect the stage (advanced) and location of the tumor.[4] Inappetence without vomiting may indicate colon cancer and is often a late sign, as appeared to be the situation in macaque 2. Other signs such as change in fecal diameter, constipation, diarrhea, and abdominal discomfort may also be noted.[4]

Several reports have characterized the diagnosis, clinical, and histopathologic presentation of intestinal adenocarcinoma in rhesus macaques.[13,16,22,25,26,30] The cases described here correlate well with these published findings. As in case 1, survey radiography may reveal fluid or gas distention of the gastrointestinal tract proximal to the tumor suggesting obstructive disease. In both cases, barium studies may have revealed annular constrictions of the intestine. We elected not to use barium in case 1 in light of the significant risk of aspiration pneumonia secondary to emesis. Routine diagnostics in case 2 included ultrasonography, which permitted direct visualization of the tumor and fine-needle aspiration. Ultrasonography may also be useful in cases in which a discrete tumor cannot be found. A thickened intestinal wall with loss of layering may be evident and suggests transmural invasion.[15] However, a gas-filled bowel or fluid-distended stomach can preclude complete visualization of the gastrointestinal tract, as was our experience.

Hematology may reveal a microcytic hypochromic anemia with a reactive thrombocytosis, suggesting iron-deficiency anemia. Iron-deficiency anemia in female rhesus macaques may occur secondary to prolonged or particularly heavy menstrual cycles. If menorrhagia is not the cause, then chronic gastrointestinal blood loss should be investigated. The anemia in our ovariectomized female macaque may have been secondary to chronic inflammatory disease or due to gastrointestinal bleeding secondary to the tumor. We suspect that fecal occult blood tests may have been negative because bleeding was intermittent and because of the lack of fresh samples for testing. Fecal occult blood tests are only moderately sensitive and should be performed on fresh or

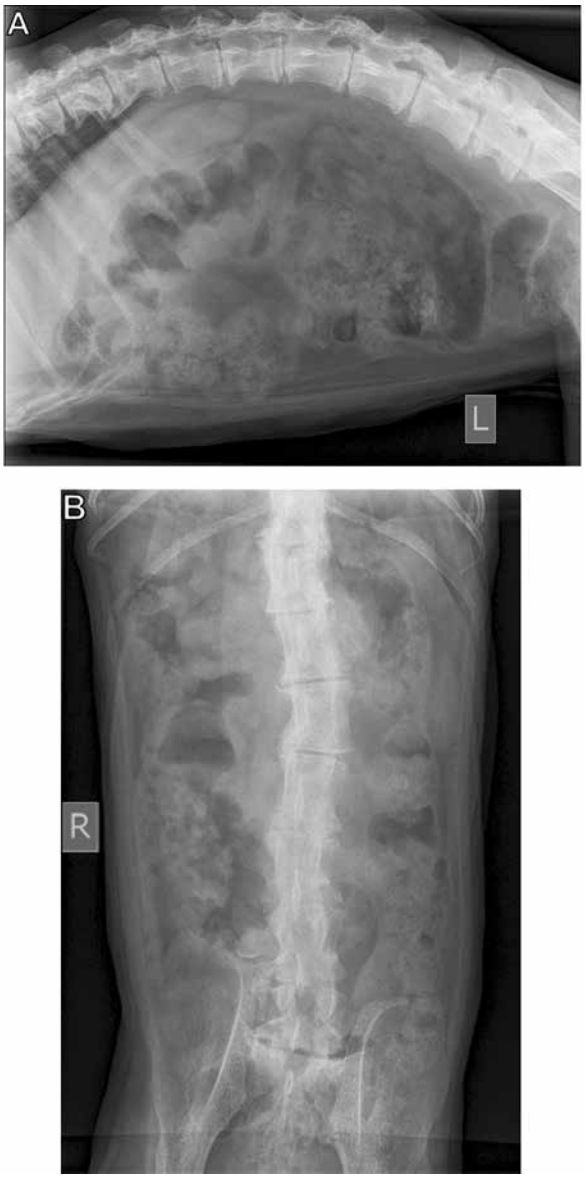

Figure 4. Abdominal radiographs of rhesus macaque 2. (A) Lateral and (B) ventrodorsal views demonstrate a diffusely enlarged and dilated colon; images were taken 6 mo prior to necropsy. Kyphosis secondary to spinal osteoarthritis is present.

rehydrated stool to increase sensitivity.[4] In humans with colon cancer, hypoalbuminemia typically reflects decreased synthesis and is associated with increased postoperative complications and delayed recovery.[4,18] The combined effects of hepatic involvement, chronic gastrointestinal bleeding, and inflammation may have led to the hypoalbuminemia seen in macaque 2. The animal in case 1 may also have been hypoalbuminemic, but this condition may not have been reflected biochemically because of dehydration. Given the proximal location of this animal's cancer, intestinal malabsorption would be a likely contributor to a low albumin, in addition to inflammation. The electrolyte abnormalities encountered were likely due to a combination of upper gastrointestinal obstruction and metabolic acidosis. In addition, as seen in case 1, moderate to frequent emesis often accompanies small bowel obstruction. Moreover, emesis progressing to feculent fluid, a result of bacterial fermentation in stagnant bowel, is further evidence of obstructive disease.

With the exception of the fine-needle aspirate, all of the aforementioned diagnostics are based solely on morphology. Histopathology is necessary for a definitive diagnosis. In macaques, adenocarcinoma most commonly occurs at the cecum, ileocecal junction, and proximal colon, thereby limiting the value of endoscopy.[22,25] Colonoscopy may be an option in some instances, but fecaliths within diverticuli, as seen in macaque 2, may impede visualization and attempts at biopsy. Therefore exploratory laparotomy is often necessary to obtain full-thickness biopsies and assess any potential local invasion of cancer. However, rhesus macaques with adenocarcinoma are frequently geriatric and may have comorbidities, discouraging clinicians from embarking on exploratory surgery without strong evidence of malignancy. Noninvasive high-resolution imaging capable of identifying anatomical sites of disease are preferred over invasive diagnostic techniques, particularly in cases in which there is a high level of suspicion but no palpable mass. Human studies have shown that 2-[^{18}F]fluoro-2-deoxy-d-glucose FDG-PET–CT is useful for detecting neoplasms of the intestines incidentally and before the onset of clinical signs.[12,23,24]

PET is used most commonly to image the activity of an injected radiopharmaceutical, 2-[^{18}F]FDG, as a means to discriminate benign from malignant tissues. FDG is a glucose analog in which the positron-emitting radioactive isotope ^{18}F is substituted for the normal hydroxyl group at the 2′ position in the glucose molecule. Its utility relies on the fact that malignant tissue typically exhibits markedly increased rates of glucose metabolism.[3,11,23] FDG, like glucose, is actively transported into cells mediated by glucose transport proteins.[3,11,19,23] Once intracellular, both glucose and FDG undergo the initial step of glycolysis, phosphorylation by hexokinase. Because the 2′ hydroxyl group of the glucose molecule is needed for further glycolysis, glucose is able to proceed through the glycolytic pathway, whereas FDG becomes trapped intracellularly. Consequently, the distribution of FDG is reflective of the distribution of glucose cellular uptake and subsequent phosphorylation. FDG-6-phosphate cannot move out of the cell, and radioactive decay ensues. Energy emitted from this decay is detected and recorded to produce PET images.

FDG decay occurs through the emission of positrons (that is, β decay).[3] Once emitted, the positron travels 1 to 3 mm, losing energy to tissues. When most of its energy is lost, a positron reacts with an electron, resulting in the emission of 2 high-energy photons in opposite directions approximately 180 degrees from each other, a process known as annihilation.[3,11] Within the scanner, each photon interacts with the PET detector ring defining a line of response within the body along which annihilation occurred. This line defines a tissue site where positron emission occurred, that is, a site of FDG activity. The simultaneous detection of the 2 photons is called coincidence; the coincidence events detected during an imaging period are recorded by the PET computer system.[3] This data is then reconstructed by a computer, producing cross-sectional images in the axial, sagittal, and coronal planes. The CT and PET data sets then are coregistered electronically by dedicated software. The data can then be viewed simultaneously as CT data, PET data, or both (superimposed) in any percentage combination.

Attributes of tumor cells favoring glucose and FDG uptake include increased numbers of glucose transporters, high levels of

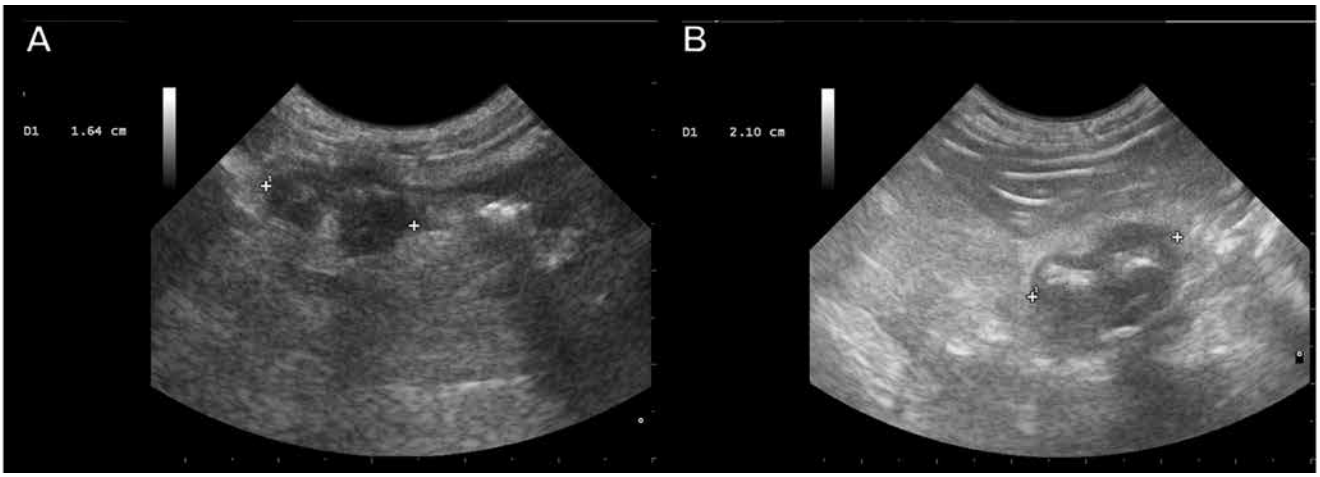

Figure 5. Abdominal ultrasonography of macaque 2. Images were taken 6 mo prior to necropsy. The continuous hypoechoic pattern suggests that the cranial abdominal mass is associated with the intestines. (A) Cranially, the mass is 1.64 cm in diameter; (B) caudally, the mass is 2.10 cm in diameter.

hexokinase, and high mitotic rates.[11] Although PET–CT with FDG has been shown to be sensitive in the detection of many malignancies, its specificity is low because FDG activity is seen both physiologically and in infectious and inflammatory processes.[3,9,24] Sites of normal physiologic uptake of FDG include brain, heart, liver, bone marrow, and urinary tract. Nonneoplastic causes of focal FDG uptake within the bowel include, inflammatory bowel disease, appendicitis, diverticulitis, and abdominal or pelvic abscesses.[3,9,28] The appearance of these lesions on CT is well described, and with experience, should not be confused with neoplasia.[24] Monitoring of inflammatory diseases is another valuable use of FDG-PET–CT, because FDG activity has been shown to decrease with successful treatment of inflammatory bowel disease.[6,28]

The ability of FDG-PET to detect tumors is dependent on many factors including histology (FDG avidity), volume, and physiologic uptake in adjacent background. Generally, due to the limits of spatial resolution, sensitivity declines with tumors smaller than 1 cm.[17,21] Although FDG-PET is highly sensitive in the detection of liver metastases,[21] we suspect that in case 2, both the lung and liver metastases may have been absent at the time of imaging, which occurred 6 mo prior to necropsy. Tumors that are generally not FDG-avid include bronchoalveolar carcinomas, carcinoid tumors of the lung, renal cell carcinomas, and low-grade lymphoma. Mucinous adenocarcinomas are known to produce false-negative results.[7,21] Three recent studies reported a 22% to 25% incidence of mucinous adenocarcinoma among macaques diagnosed with intestinal adenocarcinoma.[25,26] However, in a recent human case report, a very small focus of metastatic mucinous adenocarcinoma was detected, proving that PET–CT does have value in detecting these types of cancers.[7]

The most significant pitfall in interpreting FDG-avid foci relating to bowel is intestinal motility. Physiologic uptake in the bowel is thought to be secondary to metabolically active smooth muscle and mucosa, swallowed secretions, or microbial uptake.[1,9,19,24] Generally, tumors present as shorter-segment, more focally intense lesions, whereas nonmalignant lesions are longer.[6,12,24] This characteristic was demonstrated in both cases reported here.

Despite the potential shortcomings of FDG-PET–CT, recent studies in human medicine have shown that many incidentally detected foci of FDG avidity were revealed to be malignant or premalignant lesions once they were biopsied.[8-10,29] As a result, any focus of activity more intense than that observed in physiologic background bowel activity should be suspected as neoplastic. An additional feature of FDG-PET imaging in humans that can be extrapolated to macaques is the increased endometrial activity (FDG uptake) observed during ovulation and menstruation. Because glucose competes with FDG uptake, elevated blood glucose levels may decrease the sensitivity of PET imaging and result in false negatives. In human medicine, PET–CT typically is not performed if the blood glucose exceeds 150 mg/dL.

Intestinal adenocarcinoma is the most common malignant neoplasm of aged rhesus macaques.[2,5,25,26,30] Early detection with surgical resection of the affected bowel can be curative. However, its insidious onset coupled with the stoic nature of captive macaques often precludes timely intervention. In one study, palpation and contrast radiographs were the most useful tools to support a diagnosis.[25] However, a palpable abdominal mass or radiographic evidence of disease are often late findings, as was evident in the cases reported here. In another study, aging colonies were monitored closely for signs of gastrointestinal disease and surgically explored early on as standard practice.[26] It is somewhere between these 2 extremes that FDG-PET–CT may find its niche in nonhuman primate medicine. The main advantage of this modality in human medicine is its ability to detect potential cancer foci at its early stages.[12] Admittedly, the cases we reported here were advanced. However, by reporting our use of FDG-PET–CT, we hope to bring to the forefront a noninvasive diagnostic tool with potential for early detection of lesions suspicious for intestinal adenocarcinoma. In some facilities it may be feasible to institute this modality as a potential early cancer-screening tool for aged rhesus macaques with vague gastrointestinal signs. Despite the limitations of FDG-PET–CT, the expertise of the radiologist and

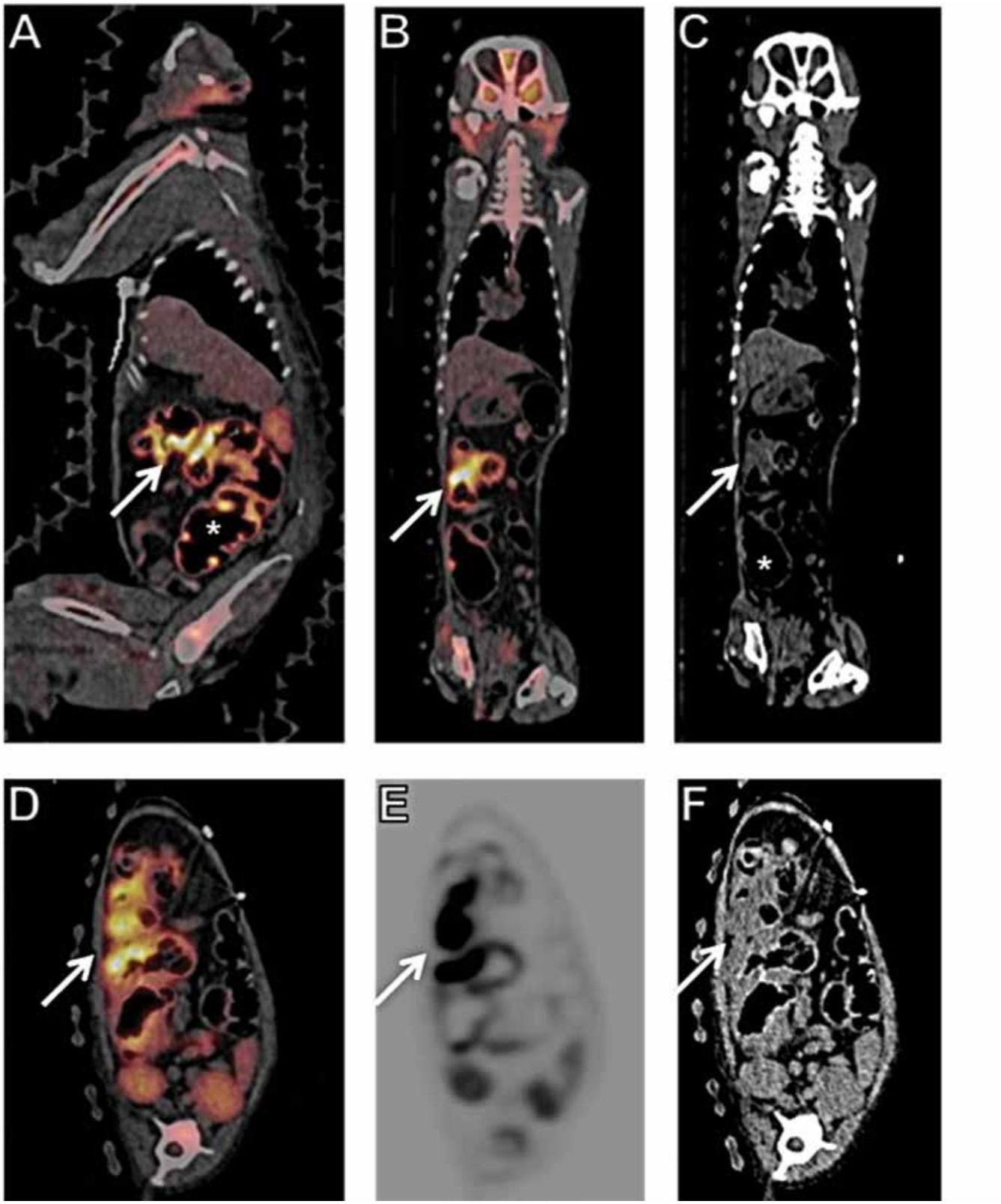

Figure 6. Whole-body FDG-PET–CT images of 2. There is focal intense FDG uptake (arrows) in an irregular transmural mass involving a segment of ascending colon just distal to the cecum. The mass causes near-complete obstruction of the lumen. The proximal bowel is dilated (*) with diffuse FDG uptake noted throughout, likely related to peristalsis or inflammation. Less-intense physiologic FDG activity is present in the brain, parotid salivary glands, liver, kidneys, and bone marrow. PET–CT (A) sagittal, (B) coronal, and (D) transaxial views; CT (C) coronal and (F) transaxial views; (E) FDG-PET transaxial view.

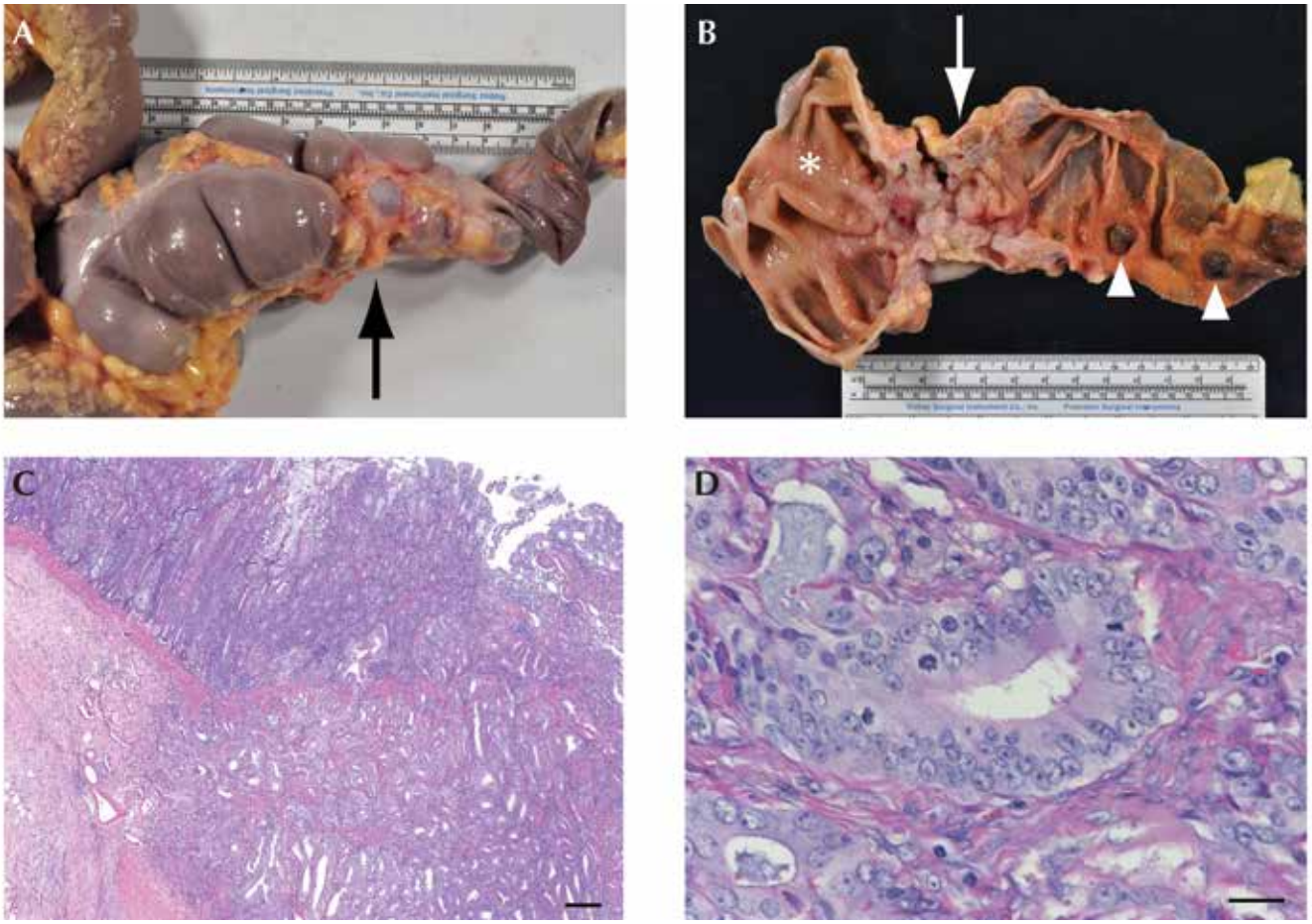

Figure 7. Gross and histologic images of intestinal mass from macaque 2. (A and B) Multinodular transmural adenocarcinoma (approximately 4 cm × 4.5 cm × 5 cm) is seen within the proximal colon just distal to the cecum (arrows). The cecum, colon, and distal small intestine are markedly dilated (left of arrow), whereas the colon distal to the neoplasm is atrophied (right of arrow). (B) On cut section, the neoplastic mass invades the intestinal wall. It is accompanied by marked desmoplasia resulting in circumferential constriction of the lumen, partial obstruction, and dilation (*) proximal to the lesion. Also note that the multiple focal diverticula located within the intestinal wall (arrowhead). (C) Histology of the mass reveals a markedly expanding, transmural and infiltrative neoplasm within the colonic wall. Neoplastic cells form tubules and acini embedded in abundant fibrous connective tissue. Hematoxylin and eosin stain; scale bar, 200 µm. (D) Neoplastic cells are columnar to polygonal with indistinct cell borders and moderate amounts of pale eosinophilic cytoplasm. Mitotic figures are prominent. Hematoxylin and eosin stain; scale bar, 20 um.

careful correlation with CT may allow the identification of early cancers routinely.

Acknowledgments

We thank Krista Fowles and Maria Corsi (Yale PET Center) for performing the PET scan, Gordon Terwilliger for necropsy support, and Arthur Nugent and Michael Schadt for their technical assistance in histologic preparations.

References

1. **Abouzied MM, Crawford ES, Nabi HA**. 2005. ^{18}F-FDG imaging: pitfalls and artifacts. J Nucl Med Technol **33:**145–155.
2. **Aristizabal-Arbelaez M, Mejia-Restrepo J, Montoya-Florez M, Grandi F, Pedraza-Ordonez F.** 2012. Immunohistochemical and morphological features of a small bowel leiomyoma in a black-crested macaque (*Macaca nigra*). BMC Vet Res **8:**97.
3. **Basu S, Kwee TC, Surti S, Akin EA, Yoo D, Alavi A.** 2011. Fundamentals of PET and PET–CT imaging. Ann N Y Acad Sci **1228:**1–18.
4. **Cappell MS.** 2005. The pathophysiology, clinical presentation, and diagnosis of colon cancer and adenomatous polyps. Med Clin North Am **89:**1–42 [vii.].
5. **Christian R, Abee KM, Tardif SD, Morris T.** 2012. Nonhuman primates in biomedical research 2: diseases. San Diego (CA): Academic Press.
6. **Cronin CG, Scott J, Kambadakone A, Catalano OA, Sahani D, Blake MA, McDermott S.** 2012. Utility of positron emission tomography–CT in the evaluation of small bowel pathology. Br J Radiol **85:**1211–1221.
7. **Funahashi K, Ushigome M, Kaneko H.** 2011. A role of ^{18}F-fluorodeoxyglucose positron emission–computed tomography in a strategy for abdominal wall metastasis of colorectal mucinous adenocarcinoma developed after laparoscopic surgery. World J Surg Oncol **9:**28.
8. **Gutman F, Alberini JL, Wartski M, Vilain D, Le Stanc E, Sarandi F, Corone C, Tainturier C, Pecking AP.** 2005. Incidental colonic focal lesions detected by FDG PET–CT. AJR Am J Roentgenol **185:**495–500.
9. **Israel O, Yefremov N, Bar-Shalom R, Kagana O, Frenkel A, Keidar Z, Fischer D.** 2005. PET–CT detection of unexpected gastrointestinal

foci of 18F-FDG uptake: incidence, localization patterns, and clinical significance. J Nucl Med **46:**758–762.

10. **Kamel EM, Thumshirn M, Truninger K, Schiesser M, Fried M, Padberg B, Schneiter D, Stoeckli SJ, von Schulthess GK, Stumpe KD.** 2004. Significance of incidental 18F-FDG accumulations in the gastrointestinal tract in PET–CT: correlation with endoscopic and histopathologic results. J Nucl Med **45:**1804–1810.
11. **Kapoor V, McCook BM, Torok FS.** 2004. An introduction to PET–CT imaging. Radiographics **24:**523–543.
12. **Kei PL, Vikram R, Yeung HW, Stroehlein JR, Macapinlac HA.** 2010. Incidental finding of focal FDG uptake in the bowel during PET–CT: CT features and correlation with histopathologic results. AJR Am J Roentgenol **194:**W401–W406.
13. **Kerrick GP, Brownstein DG**. 2000. Metastatic large intestinal adenocarcinoma in 2 rhesus macaques (*Macaca mulatta*). Contemp Top Lab Anim Sci **39:**40–42.
14. **Kim JI, Lee Y, Lee J, Jeong S, Chung H, Han J.** 2012. Use of ^{18}F-fluorodeoxyglucose positron emission tomography–computed tomography in a miniature pig (*Sus scrofa domestica*) with pneumonia. Comp Med **62:**203–208.
15. **Larson MM, Biller DS.** 2009. Ultrasound of the gastrointestinal tract. Vet Clin North Am Small Anim Pract **39:**747–759.
16. **Lembo TM, Tinkey PT, Cromeens DM, Gray KN, Price RE.** 1997. Stenosing colonic adenocarcinoma in a female rhesus monkey. J Med Primatol **26:**229–232.
17. **Lim HS, Yoon W, Chung TW, Kim JK, Park JG, Kang HK, Bom HS, Yoon JH.** 2007. FDG PET–CT for the detection and evaluation of breast diseases: usefulness and limitations. Radiographics **27 Suppl 1:**S197–S213.
18. **Lohsiriwat V, Chinswangwatanakul V, Lohsiriwat S, Akaraviputh T, Boonnuch W, Methasade A, Lohsiriwat D.** 2007. Hypoalbuminemia is a predictor of delayed postoperative bowel function and poor surgical outcomes in right-sided colon cancer patients. Asia Pac J Clin Nutr **16:**213–217.
19. **Long NM, Smith CS**. 2011. Causes and imaging features of false positives and false negatives on 18F-PET–CT in oncologic imaging. Insights Imag **2:**679–698.
20. **Marini RP, Muthupalani S, Shen Z, Buckley EM, Alvarado C, Taylor NS, Dewhirst FE, Whary MT, Patterson MM, Fox JG.** 2010. Persistent infection of rhesus monkeys with '*Helicobacter macacae*' and its isolation from an animal with intestinal adenocarcinoma. J Med Microbiol **59:**961–969.
21. **O'Connor OJ, McDermott S, Slattery J, Sahani D, Blake MA.** 2011. The use of PET–CT in the assessment of patients with colorectal carcinoma. Int J Surg Oncol **2011:**846512.
22. **O'Sullivan MG, Carlson CS.** 2001. Colonic adenocarcinoma in rhesus macaques. J Comp Pathol **124:**212–215.
23. **Okuno T, Fu K-I, Sano Y, Yoshino T, Murakami K, Ochiai A, Yoshida S.** 2004. Early colon cancers detected by FDG-PET: a report of 2 cases with immunohistochemical investigation. Hepatogastroenterology **51:**1323–1325.
24. **Prabhakar HB, Sahani DV, Fischman AJ, Mueller PR, Blake MA.** 2007. Bowel hot spots at PET–CT. Radiographics **27:**145–159.
25. **Rodriguez NA, Garcia KD, Fortman JD, Hewett TA, Bunte RM, Bennett BT.** 2002. Clinical and histopathological evaluation of 13 cases of adenocarcinoma in aged rhesus macaques (*Macaca mulatta*). J Med Primatol **31:**74–83.
26. **Simmons HA, Mattison J.** 2011. The incidence of spontaneous neoplasia in 2 populations of captive rhesus macaques (*Macaca mulatta*). Antioxid Redox Signal **14:**221–227.
27. **Sleisenger MH, Fordtran JS.** 2010. Sleisenger and Fordtran's gastrointestinal and liver disease: pathophysiology, diagnosis, management, vol 2. Philadelphia (PA): Saunders–Elsevier.
28. **Spier BJ, Perlman SB, Jaskowiak CJ, Reichelderfer M**. 2010. PET–CT in the evaluation of inflammatory bowel disease: studies in patients before and after treatment. Mol Imaging Biol **12:**85–88.
29. **Tatsumi M, Nakamoto Y, Traughber B, Marshall LT, Geschwind JF, Wahl RL**. 2003. Initial experience in small animal tumor imaging with a clinical positron emission tomography/computed tomography scanner using 2-[^{18}F]fluoro-2-deoxy-D-glucose. Cancer Res **63:**6252–6257.
30. **Valverde CR, Tarara RP, Griffey SM, Roberts JA.** 2000. Spontaneous intestinal adenocarcinoma in geriatric macaques (*Macaca* spp.). Comp Med **50:**540–544.